References

BEYERS, R., KIM, K. B. & SINCLAIR, R. (1987). *J. Appl. Phys.* **61**, 2195-2202.

BOVIN, J. O., WALLENBERG, R. & SMITH, D. J. (1986). *Nature (London)*, **317**, 47-49.

BUTLER, E. P. & HALE, K. F. (1981) *Practical Methods in Electron Microscopy*, Vol. 9, edited by A. M. GLAUERT, pp. 1-457. Amsterdam: North-Holland.

COWLEY, J. M. & IIJIMA, S. (1972). *Z. Naturforsch. Teil A*, **27**, 445-449.

EYRING, L., DUTNER, C., GORAL, J. P. & HOLLADAY, A. (1985). *Ultramicroscopy*, **18**, 253-274.

GIBSON, J. M., MCDONALD, M. C. & UNTERWALD, F. C. (1985). *Phys. Rev. Lett.* **55**, 1765-1767.

HASHIMOTO, H., TAKAI, Y., YOKOTA, Y., ENDO, H. & FUKUTA, E. (1980). *Jpn. J. Appl. Phys.* **19** L1-L4.

HOLLOWAY, K. & SINCLAIR, R. (1987). *J. Appl. Phys.* **61**, 1359-1364.

HOLLOWAY, K. & SINCLAIR, R. (1988*a*). *J. Less-Common Met.* **140**, 139-148.

HOLLOWAY, K. & SINCLAIR, R. (1988*b*). *Proc. Mater. Res. Soc.* **103**, 167-172.

HORNSTRA, J. (1958). *J. Phys. Chem. Solids*, **5**, 129-141.

IIJIMA, S. & ICHIHASHI, T. (1986). *Phys. Rev. Lett.*, **56**, 616-618.

KANG, Z. C. & EYRING, L. (1987). *Ultramicroscopy*, **23**, 275-281.

KIM, K. B., KNIFFIN, M., SINCLAIR, R. & HELMS, C. R. (1988). *J. Vac. Sci. Technol.* A**6**, 1473-1477.

LAHAV, A., EIZENBERG, M. & KOMEM, Y. (1985). *Proc. Mater. Res. Soc.* **37**, 641-646.

LAHAV, A., EIZENBERG, M. & KOMEM, Y. (1987). *J. Appl. Phys.* **62**, 1768-1777.

LU, P. & SMITH, D. J. (1987). *Phys. Rev. Lett.* **59**, 2177-2179.

MAEDA, K., SATO, M., KUBO, A. & TAKEUCHI, S. (1983). *J. Appl. Phys.* **54**, 161-168.

MAEDA, K., SUZUKI, K., ICHIHARA, M. & TAKEUCHI, S. (1984). *J. Appl. Phys.* **56**, 554-556.

MAEDA, K. & TAKEUCHI, S. (1983). *Appl. Phys. Lett.* **42**, 664-668.

MARKS, L. D. (1983). *Phys. Rev. Lett.* **51**, 1000-1002.

MARKS, L. D. & SMITH, D. J. (1983). *Nature (London)*, **303**, 316-318.

MENTER, J. W. (1956). *Proc. R. Soc. London Ser. A*, **236**, 119-129.

OGAWA, M. (1980). *Thin Solid Films*, **70**, 181-189.

OPYD, W. G., GIBBONS, J. F., BRAVMAN, J. C. & PARKER, M. A. (1986). *Appl. Phys. Lett.* **49**, 974-976.

PARKER, M. A. (1988). *In Situ High-Resolution Transmission Electron Microscopy of Solid-Phase Epitaxy in Silicon and Silicon on Sapphire.* PhD thesis. Stanford Univ., USA.

PARKER, M. A. & SINCLAIR, R. (1985). *Proc. Electron Microsc. Soc. Am.* **43**, 358-359.

RAAIJMAKERS, I. J. M. M., READER, A. H. & VAN HOUTUM, H. J. W. (1987). *J. Appl. Phys.* **61**, 2527-2532.

SANDS, T., KERAMIDAS, V. G., WASHBURN, J. & GRONSKY, R. (1986). *Appl. Phys. Lett.* **48**, 402-404.

SANDS, T., KERAMIDAS, V. G., YU, A. J., GRONSKY, R. & WASHBURN, J. (1987). *J. Mater. Res.* **2**, 262-275.

SCHRODER, H., SAMWER, K. & KOSTER, U. (1985). *Phys. Rev. Lett.* **54**, 197-200.

SINCLAIR, R. & PARKER, M. A. (1986). *Nature (London)*, **322**, 531-533.

SINCLAIR, R., PARKER, M. A. & KIM, K. B. (1987). *Ultramicroscopy*, **23**, 383-396.

SINCLAIR, R., PONCE, F. A., YAMASHITA, T., SMITH, D. J., CAMPS, B. A., FREEMAN, L. A., ERASMUS, S. J., NIXON, W. C., SMITH, K. C. A. & CATTO, C. J. C. (1982). *Nature (London)*, **298**, 127-131.

SINCLAIR, R., YAMASHITA, T. & PONCE, F. A. (1981). *Nature (London)*, **290**, 386-388.

SMITH, D. J. & BARRY, J. C. (1987). *Ultramicroscopy*, **23**, 255-478.

SMITH, D. J., PETFORD-LONG, A. K., WALLENBERG, L. R. & BOVIN, J. O. (1986). *Science*, **233**, 872-875.

YAMASHITA, T. & SINCLAIR, R. (1983*a*). *Proc. Electron Microsc. Soc. Am.* **41**, 112-113.

YAMASHITA, T. & SINCLAIR, R. (1983*b*). *Proc. Mater. Res. Soc.* **14**, 295-298.

Acta Cryst. (1988). A**44**, 975-986

Signal Processing of High-Resolution Transmission Electron Microscope Images Using Fourier Transforms

BY P. R. BUSECK

Departments of Geology and Chemistry, Arizona State University, Tempe, Arizona 85287, *USA*

AND Y. EPELBOIN AND A. RIMSKY

Universités P. M. Curie et Paris 7, *UA* 009 *CNRS*, 4 *place Jussieu*, 75252 *Paris CEDEX* 05, *France*

(*Received* 3 *February* 1988; *accepted* 22 *June* 1988)

Abstract

Interpretation of images obtained by high-resolution transmission electron microscopy (HRTEM) can be aided by the use of processed signals. Images are recorded digitally or are digitized from a photograph, and then these data are Fourier transformed and treated. The low- and high-frequency signals are removed, and a variety of circular and elliptical (anisotropic) apertures or screens are applied to explore and highlight features of special interest. A minicomputer can be used to perform such image processing rapidly, interactively, and with high precision. Elliptical filters are of special interest for the examination of linear or planar features such as the distribution of stacking faults or the presence and distribution of superstructures. Some superstructures themselves contain defects, and these can similarly

0108-7673/88/060975-12$03.00

be highlighted and examined. The uses of processing for examining HRTEM images of layering in a complex sheet silicate mineral and dislocation cores in grossular garnet are illustrated.

1. Introduction

The advent of high-resolution transmission electron microscopes in laboratories worldwide has resulted in abundant images of crystals that show details down to the atomic level. Interpreting such images can be difficult, and the problems increase as the instrumental resolution improves. Part of the difficulties lie in the image-forming process itself, but complexities also occur in unravelling the substantial information content of high-resolution images. In this paper we address the second question and show how image-analysis procedures can be used to aid in the interpretation of complex images.

There is an extensive literature on signal processing and image analysis, and a less-extensive one on its application to high-resolution transmission electron microscopy (HRTEM). Thorough reviews of the general problems and procedures are provided in the books by Castleman (1977) and Saxton (1978), and Saxton, Pitt & Horner (1979) have written a program (*SEMPER*) to process digital images. Sattler & O'Keefe (1987) have used Fourier filtering to improve the images of small particles, and Saxton (1986) has used processed images and digital filters of different types to improve high-resolution images, as have Pradre, Revol & Manley (1987). Yokota, Tomita, Hashimoto, & Endoh (1981) built an on-line processing machine, but it is not as versatile as using a computer for treating images.

The use of Fourier transforms to process images is relatively common (*e.g.* Gonzales & Wintz, 1977), although the lack of easily accessible fast computers has limited their use. When doing electron microscopy, it is common to select particular diffraction spots to emphasize certain components of the image, and this is done in the microscope when producing the image. Our aim is to enhance the contrast of an image that has already been obtained in the TEM and to highlight features of interest. Moreover, only isotropic filters (circular or annular apertures centered on the origin) are generally used in calculations, and these are also the only ones used directly in the TEM. We suggest that for analysis of HRTEM images anisotropic filters can be of great use, as discussed below.

The goals of this paper are (*a*) to describe the principles underlying such digital signal processing, especially using anisotropic filters, and (*b*) to provide examples of their applications to problems in crystallography and specifically to the study of defects in minerals. An important feature of such processing is that it permits a more objective interpretation of the image than is commonly provided by simple visual observation. Any minimization of subjectivity in image interpretation is useful. Moreover, a great variety of filter types and combinations can be applied rapidly and without experimental difficulties to a given image to extract various types of information.

2. Image treatment

The study of any image is complex, and the procedures for image processing described here are quite general. The process is summarized in Fig. 1. The main problems are discussed at the various stages of image treatment, and a detailed explanation is given by Rimsky, Epelboin & Morris (1988).

2.1. *Image data acquisition*

Selection of optimal operating conditions for obtaining a good TEM image depends on proper instrument alignment (Smith, Saxton, O'Keefe, Wood & Stobbs, 1983), good sample stability (Hobbs, 1979, 1983; Veblen & Buseck, 1983), and considerable operator skill and experience. However, even under the best of circumstances, potentially serious distorting effects can arise. These effects may be produced by spatial aberrations (*e.g.* chromatic and spherical aberrations, defocus, electron-beam coherence) and anamorphosis (resulting from different magnifications in perpendicular directions) in the image. Some of these effects can be corrected by numerical treatment.

The transfer function that describes the modification of the initial information from the exit

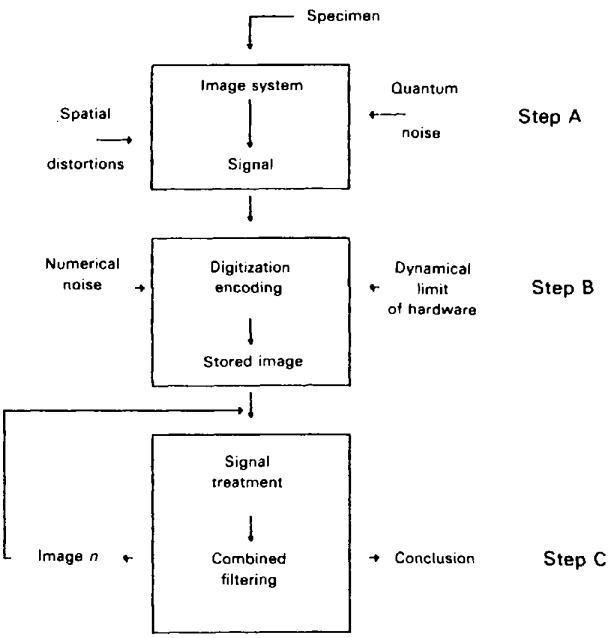

Fig. 1. Principles of image analysis.

surface of the sample into the final observation can also result in distorting effects. The transfer function can be divided into effects produced by the instrument and by diffraction. We concern ourselves here with the instrumental effects, including those produced by the lens aberrations and the defects in the electron source. The effects resulting from diffraction and image formation are discussed by, for example, Saxton (1978).

The transfer function of the instrument, the electron microscope in our case, is strongly influenced by the operating conditions. Random quantum noise accumulates unavoidably during image acquisition. It arises from both the TEM and the recording medium such as, for example, the photographic emulsion, and it blurs the image. To produce an optimal signal, the noise must be minimized at each step of the process.

2.2. *Digitization*

The intrinsic limitations of the digitizing device, associated electronics and computer are critical for final interpretation of the image. The quality of the digitization depends on both spatial sampling and the dynamic range of the signal, including the characteristics of the recording camera. Spatial sampling is determined by the size of the pixel relative to the magnification of the image. The resolution of the digitized image should be adjusted so that the spatial sampling is comparable to the resolution of the original experimental image. In order to preserve the original resolution, the sampling of the digitized image should be half the smallest period of the experimental image (Shannon, 1948).

Also important is the dynamical encoding per pixel, that is, obtaining the maximum possible range of gray levels. Each unit of data is coded in the computer on a given number of bits, which we shall call NBITS, and which is dependent on the digitizing hardware. For the illustrations in this paper, each pixel is coded on eight bits (NBITS = 8), meaning that the dynamical range is limited to 256 levels. Devices are also available that use 12 bits (Sattler & O'Keefe, 1987) or more, and scanner imaging in medical radiography uses 24 bits. In our case, the image is stored in the computer as a set of N integers, each of length NBITS, where N is the total number of pixels in the image.

Brillouin (1959) and Bijaoui (1981) characterize the image contents, C_0, by

$$C_0 = N \log_2 (2^{\mathrm{NBITS}}) = N \times \mathrm{NBITS}.$$

If one assumes that the probability of occupation of each pixel is identical, C_0 yields the maximum contents that can be stored in the image. The best digitization is achieved by decreasing the pixel size (increasing N) and by encoding each component of the signal on the greatest number of bits (increasing NBITS).

The price of the hardware and computer time are limitations; we have found that 512×512 pixels with NBITS = 8 is satisfactory. If greater resolution is required (and if it is available on the original image), then it is possible to increase the optical magnification of the image during digitization and to treat the image in parts.

2.3. *Image processing*

At this step it is desirable to decrease or, if possible, eliminate the noise that was introduced in the preceding steps. Following that, image processing depends on the desired goals. Contrast may be enhanced to permit examination of features of special interest, or else particular structures or parts of structures may be extracted for study. The latter operation is more delicate since in order to apply the proper digital filters (described below) the operator needs to have prior knowledge of the structural features to be examined. For example, if particular sets of atoms in a HRTEM image are to be examined, it is necessary to know their possible orientations before they can be highlighted and studied.

3. Data acquisition

The quality of a digitized image depends on how the image is digitized and how the noise, intrinsic to the acquisition of any signal, is minimized. These are discussed below.

3.1. *Information rate in an image*

An ideal recorder collects events independently of one another, which is what occurs for photons collected in a pixel. Great care must be used during image acquisition; if insufficient information to achieve the desired goal is contained in the image, the processing cannot produce significant results.

Statistically, the photons follow a Poisson distribution. However, in order to simplify the calculations we will utilize a Laplacian-Gaussian distribution. This does not seriously affect the result. Felgett & Linfoot (1955) have studied the information lost by a Gaussian perturbation arising from noise in frequency space. Let us consider a given spatial frequency ν and two variables, $\sigma_s(\nu)$ and $\sigma_n(\nu)$ which are the variances of the signal, s, and noise, n, respectively.

The information rate for the fequency, $I(\nu)$, may be written as

$$I(\nu) = \tfrac{1}{2} \log_2 [1 + \sigma_s(\nu)/\sigma_n(\nu)]. \qquad (1)$$

Thus, the information rate increases in proportion to the log of the variance of the signal-to-noise ratio.

The noise varies both temporally and spatially in the image. Its dispersion is characterized by a probability function, $p(\nu)$. Let us define $\sigma'_n(\nu)$ as

$$\sigma'_n(\nu) = p^2(\nu)\sigma_n(\nu),$$

and so (1) becomes

$$I(\nu) = \tfrac{1}{2}\log_2 [1 + \sigma_s(\nu)p^2(\nu)/\sigma'_n(\nu)]. \quad (2)$$

Since the image is digitized into $2L$ pixels along a row or column, the range of known frequencies in Fourier space is sampled on $2L$ different values. The sampling step $\delta(\nu)$ in frequency space is

$$\delta(\nu) = 1/2L.$$

The density of information $J(\nu)$ in an image may be defined as

$$J(\nu) = \int_{-\infty}^{+\infty} I(\nu)\, d\nu,$$

which is the product of the information rate and sampling step. Then it follows from (2) that

$$J(\nu) = (1/4L) \sum_{-\infty}^{+\infty} \log_2 [1 + \sigma_s(\nu)p^2(\nu)/\sigma'_n(\nu)]. \quad (3)$$

The density of information increases as the dispersion of the noise decreases and the signal intensity increases. Thus, the image is characterized by the spatial sampling (the dimensions of the pixel and thus the step size) and by the quality of the information in each pixel (*i.e.* the signal-to-noise ratio plus the magnitude of the signal). It is therefore desirable to utilize the full dynamic range of the recording camera, which means that the range of values for each pixel must vary from zero to the maximum possible value, 255 in our case. Of course the sampling step of the digitizing device must be comparable to the spatial resolution of the original TEM image if all details are to be retained. Moreover, if the signal-to-noise ratio in the experimental image is too small, then image processing and interpretation can be hazardous and result in mistakes.

3.2. *Influence of noise*

Consider a given point on the image. When the signal from that point is recorded by the detector, we assume that it is perturbed by a noise with variance σ_s. The signal intensity i, when measured for this point, follows a Gaussian distribution. The probability of occupation of intensity level i is

$$p(i) = [(2\pi e)^{1/2}\sigma_s]^{-1} \exp [(i - \delta i)^2/2\sigma_s^2]$$

where δi is the shift from the central position of the Gaussian distribution.

By analogy with thermodynamics, an information entropy of the signal E can be defined as

$$E = -\sum p_i \log p_i,$$

where p_i is the probability of event i. The entropy of information of the digitized signal is given by Brillouin (1959) as

$$E_s = \tfrac{1}{2}\sigma_s \log (2\pi e) \quad (4)$$

where σ_s is the variance of the total image and so a function of the position of the pixel within the image. The signal is fully determined when $\sigma_s = 0$.

In the same manner we define σ_n and E_n as the corresponding values for the variance and entropy of the noise that disturbs the signal, and y as the intensity of the noise. Then

$$p(y) = [(2\pi e)^{1/2}\sigma_n]^{-1} \exp [(y - \delta y)^2/2\sigma_n^2]$$
$$E_n = \tfrac{1}{2}\sigma_n \log (2\pi e).$$

The probability that a noise of intensity level y disturbs a signal of intensity level i is

$$p(y, i) = [(2\pi e)^{1/2}\sigma_n]^{-1} \exp \{-[(y - i)^2/2\sigma_n^2]\}$$

and the variance of the signal (during digitization) is

$$\sigma_y = (\sigma_s^2 + \sigma_n^2)^{1/2}.$$

We can now express the entropy of a signal that has been affected by noise (Bijaoui, 1981) as

$$E_n = \tfrac{1}{2}\log [1 + (\sigma_s^2/\sigma_n^2)]. \quad (5)$$

It follows from the above that (*a*) for an optimal signal the noise must be minimized, and (*b*) for proper treatment the noise must be determined at each step of image processing, from initial signal acquisition through final digitization.

3.3. *Digitization*

Decreasing the noise during image acquisition (§ 3.1) is not easy. The experimental conditions are commonly determined by the sample itself and by the desired resolution and thus the instrument used. During digitization (§ 3.2), on the other hand, it is possible to decrease the noise by increasing the number of events collected into each pixel. For example, consider a digitizer that contains 512×512 pixels. The high-sensitivity camera that we use can collect roughly 500 photons in each pixel in a single video frame (in 1/25 s in Europe and 1/30 s in the US). The result is an uncertainty of approximately $\pm(500)^{1/2}$, which equals 22 photons or ±4·5%.

Assume that each pixel is stored on eight bits, that is, 256 levels. The uncertainty is then $256 \pm (4{\cdot}5\%)$ or roughly 23 levels, which means that the actual number of dynamic levels is reduced to only 11 independent gray levels. However, the dynamics can be enhanced greatly if we sum over q frames, assuming that q is sufficiently large. Thus, if the noise is decreased by $q^{1/2}$, with $q = 32$, the dynamic range becomes roughly 32 independent gray levels, which is a significant increase. However, one must be careful to remain in the range where the dynamics of the camera are linear.

4. Image processing

4.1. *Introduction*

At this stage of the process, the image is stored as a matrix that has n_1 rows and n_2 columns, with intensity $I(r)$ at each point r and with each piece of data written onto a word of length NBITS. The number of pixels is $N = n_1 n_2$. The several steps during processing are summarized in Fig. 2.

The first step is computation of the Fourier transform of the data matrix. Then a digital filter is applied in Fourier (reciprocal) space, as described below. Calculation of the inverse Fourier transform of the resulting data set produces a transformed processed image that can then be displayed on a TV monitor or accessed in other ways, as desired.

Several options are possible at this stage: (*a*) processing can be terminated; (*b*) a different digital filter can be applied to this new image; or (*c*) the entire process can be restarted using the raw data set if the applied filter is not adequate. Once the treated image is roughly acceptable, it is possible either to perform additional enhancement or to search for special features.

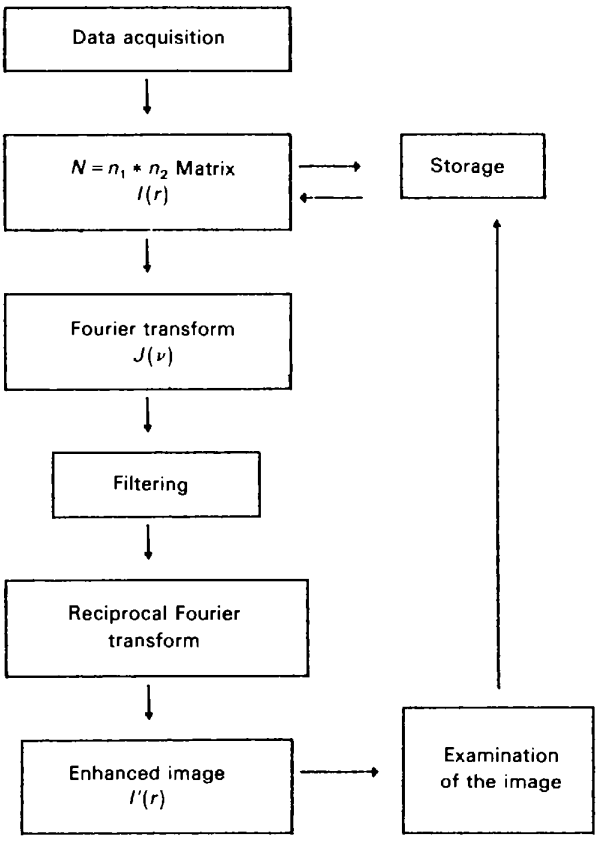

Fig. 2. Principles of digital image filtering.

4.2. *Image enhancement*

Several enhancement procedures can be applied to an image. It is possible to decrease the intrinsic noise of the image, including the grain size of the photographic emulsion, by suppressing the high frequencies. The contrast in the sample may vary slowly across the image. This effect commonly results from a variation in thickness across the sample or from instrumental and experimental factors. Such gradual differences, from low to high contrast in the image, correspond to low frequencies in Fourier space. To minimize such contrast changes, it is necessary to use a radial filter that may be a circular screen, a hole, or a combination of the two. This filter can be made partially transparent by introducing an attenuation coefficient. When applying such filters it is important to avoid removing genuine intrinsic changes in image character.

An optimum filter (Tournarie, 1959) is used in order to avoid the secondary effects (analogous to Fresnel fringes) that could arise in Fourier space from the limiting aperture. Otherwise, such effects could appear as secondary fringes in the filtered image (Gonzales & Wintz, 1977).

Let $I(r)$ be the intensity at a given point r in the image. The Fourier transform is

$$J(\nu) = \mathrm{FT}[I(r)].$$

Applying a filter results in

$$J'(\nu) = J(\nu) \times f(\nu)$$

where $f(\nu)$ is the function that simulates the various filters.

The next step is to compute the inverse Fourier transform of the image

$$I'(r) = \mathrm{FT}^{-1}[J'(\nu)].$$

The real-complex Fourier transform is computed using the algorithm of Cooley & Tukey (1965).

It is possible to use many different types of filters. Examples are given in Fig. 3, and applications are given in § 6. We use a low-pass filter with limits of ν_1 to simulate a large aperture and thereby eliminate the high-frequency noise (Fig. 3*a*). Conversely, we use a high-pass filter with limits ν_2 that simulates a central stop to suppress low-frequency signals that produce gradual systematic variations in contrast across an image (Fig. 3*b*). When both types of filters are combined, an annular-type pass filter results. The attenuation from such a filter is illustrated in Figs. 3(*c*) and (*d*). The choice of the limits for ν_1 and ν_2 depends on the experimental conditions. Computing the cumulative histogram of the frequencies in Fourier space is of considerable assistance in determining their optimal values. These filters are discussed in greater detail by Rimsky, Epelboin & Morris (1988).

4.3. *Selection of features of special interest*

The choice of filter depends on the characteristics of the features one wishes to enhance. Use of annular filters (Figs. 3*c*,*d*) permits the enhancement of contrast at the boundaries between areas having different gray levels. Saxton (1986) has used such filters to enhance the contrast at the boundaries between substructures in the image. Such filters are also useful for highlighting grain boundaries and similar features.

The use of an anisotropic filter (Fig. 4) is ideal for enhancing contrast selectively along certain directions. As shown in § 6, we have used this procedure for studying some mineral images.

The selected filter can vary widely in size and shape. It is characterized by a pair of holes of radius R and located a distance D from the origin. Their position and orientation are set relative to a reference coordinate system (ν_x, ν_y) and are specified for orientation angles φ, α. These specifications are for Fourier space. Adjustment of D allows selection of the image periodicities that are to be sampled. R affects the resolution in the processed image along the chosen direction, given by α, in which the image is being enhanced. Details in this direction will be visible, whereas the contrast will be blurred in other directions. The resolution will decrease in directions away from the line connecting the two holes, becoming zero along the direction perpendicular to the line. As R is increased, smaller details become visible in the image.

Although the above sort of filter can be useful, the gradual change in resolution from one direction to the next can be disturbing. Moreover, it is not possible independently to adjust the resolution and the direction where it is at a maximum. Thus, when R is increased, φ is also increased. An alternative procedure is to replace the circular apertures with elliptical ones (Fig. 5); this allows adjustment of angle φ independently of the previous parameters. It is possible simultaneously to select the mean direction of enhancement, α, and to adjust φ without modifying the resolution R along α. This is the procedure that we have found most useful. Adjustment of the eccentricity, e, permits selection of preferential viewing directions as well as desired resolutions (up to the limit intrinsic to the original image). The filter is designed in the computer by specifying the semimajor and semiminor axes, R and R' ($\equiv R \times e$), of the ellipses and also the positions of their centers.

Such an elliptical filter is useful, for example, for examining dislocations in high-resolution images. The paired ellipses are oriented perpendicular to the desired set of planes, as viewed in the image. A typical

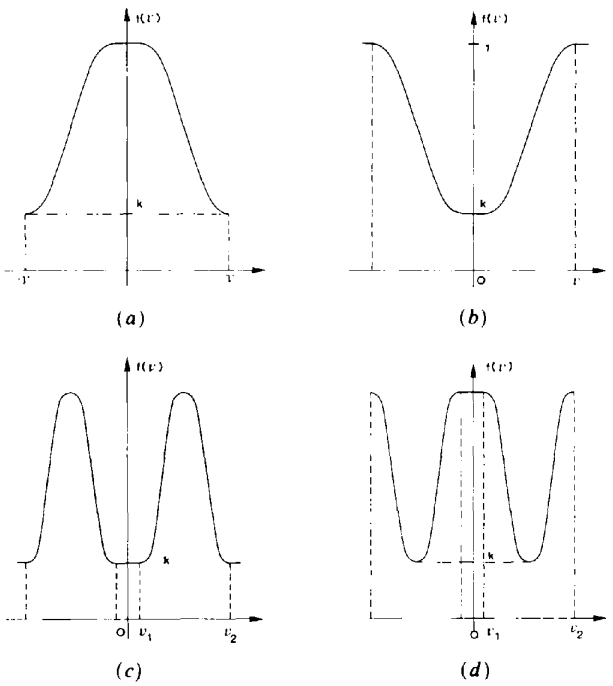

Fig. 3. Attenuation function, $f(\nu)$, for various circular aperture filters. Transmittance is plotted *vs* distance from the center of the aperture. (*a*) Low-pass filter, analogous to having a hole centered on the transmitted beam in a TEM. (*b*) High-pass filter, analogous to having a central opaque beam stop in a TEM. (*c*) Annular screen produced by a combination of (*a*) and (*b*). (*d*) Annular donut-like screen produced by the inverse of (*c*).

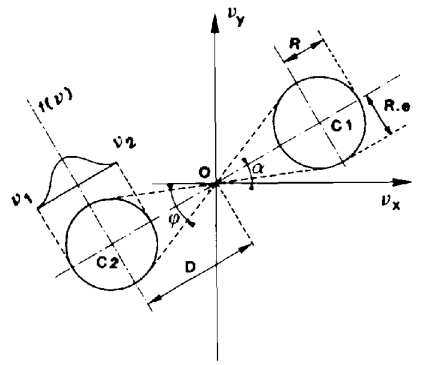

Fig. 4. Projected view of the positions and coordinates of a pair of circular apertures. The units are explained in the text.

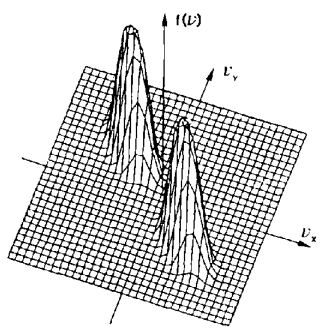

Fig. 5. A three-dimensional projection of the transmitted energy allowed to pass through an elliptical filter.

eccentricity might be 0·3. On the other hand, replacement of the holes by (digital) beam stops permits the suppression of oriented anisotropic features such as scratches.

Complete treatment of an image generally requires a selection of various filters; their details depend on the features in the initial image and the aspects desired for detailed viewing. Each filter results in the enhancement or suppression of specific types of features. A consequence is that proper interpretation of a given HRTEM image generally requires the use of several filtered images, each adapted to specific components.

Since filtering and subsequent image examination can be done digitally, and thus almost instantaneously through the use of fast Fourier transforms on a computer, it is possible to do considerable experimentation before selecting the final filtering conditions. In any case, considerable interaction between the experimentalist and the computer is both possible and necessary for the final results to be optimal images.

5. Experimental system and procedures

For the image illustrations in this paper, a Numelec Pericolor workstation is used for image analysis. It is connected to its own computer as well as to a larger Norsk system. It uses a combination of standard commercial software and dedicated software written by A. Rimsky, Y. Epelboin and colleagues. The system has mainly been used for representation of simulated X-ray topographic and electron microscope images.

The procedure is to use a Thomson video camera with a New Vicon tube to obtain a TV-rate image of a high-resolution photograph, and this is instantaneously transmitted to the adjacent Numelec system. By limiting the field of view, fall-off of camera response towards the edges of the field is negligible. The original photograph is uniformly lighted, and the illumination to the camera is adjusted (by either a diaphragm or by polarizing filters on the lens) for optimum light intensity, so that the maximum intensity in the digitized image almost corresponds to the value 255. Directly connecting the picture system to the microscope would avoid many of the problems that arise from using a photographic film.

In order to minimize statistical fluctuations, 32 images are collected in rapid sequence with the video camera. These are transmitted to the Numelec workstation and averaged. This averaged digitized image can now be processed in a variety of ways.

All filtering is done in Fourier space. The high- and low-frequency signals are identified and removed through the use of a filter applied to the digital analog of an optical diffraction pattern.

The map of the modulus of the Fourier transform, *i.e.* the digital analog of a diffractogram, clearly shows spots of various orders and, if the region is disordered, streaking. A plot is produced of intensity *vs* spatial frequency (reciprocal distance); it has peaks at spatial frequencies that correspond to the major separations in the diffractogram (and thus image). The spatial frequency at which the intensity goes to zero is generally evident, and spurious high-frequency spikes are readily identified. A digital filter is placed where the intensity goes to zero, and all higher-frequency signals are then removed (these produce much of the background noise). The lowest-frequency signals are similarly filtered out, primarily to correct the slow fluctuations in the image. Filtering the high frequencies removes the fast fluctuations such as the visibility of the grains of the emulsion or the noise.

The frequency limits of the filter to be used are determined by plotting the distribution of the modulus of the Fourier transform *vs* the signal frequency (*i.e.* the energy dispersion of the signal *vs* frequency). The selected digital filter is then applied to the diffractogram of each of the averaged images, and the inverse (reciprocal) Fourier transform is computed. The resulting filtered images have smoothed, more uniform, intensity distributions than the original images, as can be demonstrated by displaying computed intensity profiles along arbitrary traverses across the image.

Annular or circular filters are used to enhance details in regions that were either very dark or light prior to filtering. The resulting features are commonly easier to observe, and the images are aesthetically more pleasing than prior to treatment. Such filtering is preferable to the usual method of histogram equalization since the information of interest is selected without modifying the dynamics: all the fluctuations of the intensity levels in the experimental image are retained during processing.

It is now possible to inspect the image and examine features of special interest through the use of a digital (anisotropic or polar) filter. Although the shape and orientation are commonly determined from the image, the filter is applied to the Fourier transform of the image.

For elliptical filters, we generally choose a highly elongated filter that extends from the center of the diffractogram through half the radius of the screen, *i.e.* 128 pixels. The ratio of the radii of the semimajor to semiminor axes of the elliptical aperture for the figures in this paper was either 0·5 or, more commonly, 0·25. Its orientation was the main variable. Because of the reciprocal nature of the operation, fringes in the image are produced perpendicular to the long direction of the filter.

6. Mineral images

Several examples of processed images of minerals are given below. The most intricate image is that of minnesotaite, and so it receives greatest attention.

Processed images of a complex dislocation in grossularite garnet are also shown.

6.1. *Minnesotaite*

There are many sheet silicate minerals, and they have been the focus of extensive HRTEM studies. Recently, attention has been directed to minnesotaite (Guggenheim & Eggleton, 1986; Ahn & Buseck, 1988), a modulated Fe-rich silicate that is abundant in many iron ore deposits (Fig. 6*a*). It has a nominal composition of $(Fe, Mg)_{27}Si_{36}O_{86}(OH)_{26}$, which is close to that of talc, a common Mg sheet silicate. The structure is sensitive to changes in the Fe : Mg ratio, and crystals typically respond to such compositional variations by adjusting their structural elements. It is these features that are considered here.

The schematic structure projection (Fig. 6*b*) shows regions where linked SiO_2 tetrahedra project towards an adjacent sheet of octahedrally coordinated cations. Variations in composition can be accommodated by changes in the widths of the tetrahedral strips, and these are evident in images such as that in Fig. 6(*a*). Moreover, periodic variations can give rise to local superstructures and modulations, but these features can be difficult to see in the images.

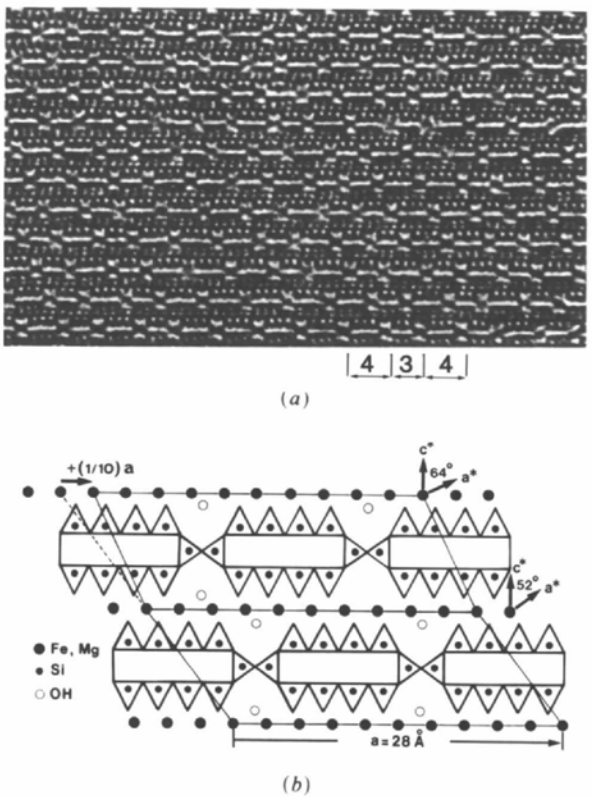

Fig. 6. HRTEM image of minnesotaite. (*a*) Strips of tetrahedrally coordinated cations appear between the rows of white spots. Variations in widths of these strips reflect subtle compositional changes, but are difficult to observe because of the amount of detail in the image. The numbers of tetrahedra in the strips at the bottom of the figure are marked. (*b*) Schematic drawing of the minnesotaite structure projected along [010]. The small triangles represent projections of tetrahedral coordination polyhedra. This projection contains strips that are four tetrahedra wide. Two alternative unit cells are marked; they indicate possible shifts by (1/10)*a* in the structural units.

It is evident from consideration of images such as Fig. 6(*a*) that an extraordinary amount of detail is present. Interpreting these details can be extremely difficult, especially since small changes in mineral thickness or TEM defocus can produce profound changes in the phases of the diffracted beams and thus in the image (O'Keefe, Buseck & Iijima, 1978; O'Keefe & Buseck 1979). Use of processed filtered images can be of assistance.

Fig. 7(*a*) shows the processed image, and the corresponding digitized Fourier transform (DFT) is shown in Fig. 7(*b*). This digitized diffractogram is analogous to an optical diffraction pattern since both correspond exactly to the region in the image. In contrast, a selected-area electron diffraction pattern obtained with a TEM generally arises from a far wider region than appears in the image.

The various apertures described in §§ 4.2 and 4.3 are applied to the DFT to examine different components of the image. In the computation of the Fourier transform, the value of the zero component is always much greater than that of the other components since it results from the integral of the entire image. To be able to visualize this Fourier transform on the screen in enhanced form, it is first necessary to remove the zero-component signal. Suppressing the zero-component signal increases the relative intensities of the other spots in the DFT and so makes small details easier to see. The use of an annular filter that suppresses both the low and high frequencies allows a simultaneous equalization of the frequency histogram and noise suppression.

Utilization of a pair of large circular filters, centered on the spots marked 2 in Fig. 7(*b*) and resulting in the two large rounded signals in Fig. 8, results in a complex image (Fig. 9*a*) that is difficult to interpret. It retains the horizontal features of the original image in Fig. 6(*a*), but it also contains prominent diagonal linear elements that were not so obvious in the original image and whose origin is not immediately apparent.

Using a smaller resolution, *i.e.* decreasing the diameter of the circular filters by a factor of 5, results in an image that contains only the diagonal features (Fig. 9*b*). Now it is evident that they represent the substructure periodicity. Cloudy regions occur where there are slight deviations in direction of these substructure fringes.

When the relatively weak superstructure spots [marked 1 in Fig. 7(*b*) and also shown in Fig. 8] are selected, the resulting image contains broad bands (Fig. 9*c*). Their wavy distribution shows that the

minnesotaite crystal is not perfectly periodic with respect to this long spacing. The cloudy regions indicate localized discontinuities, as does the apparent edge dislocation on the left.

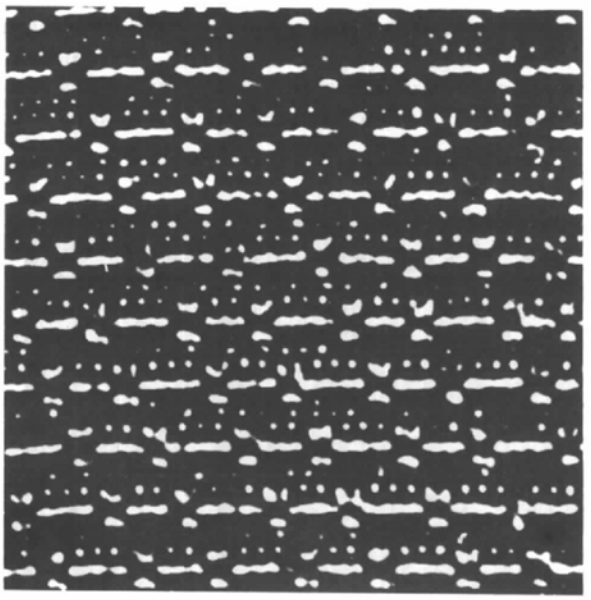

(*a*)

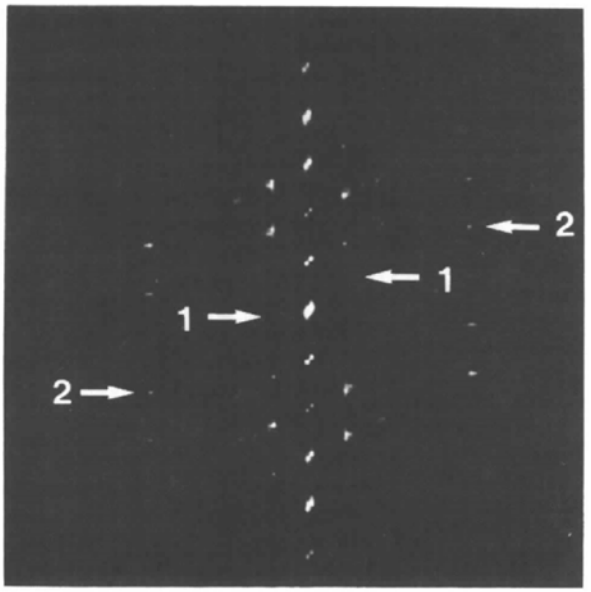

(*b*)

Fig. 7. (*a*) Processed image, obtained from part of the experimental image (Fig. 6*a*). It is the average of 32 video scans of the experimental image. The low- and high-frequency signals have been removed. (*b*) Digitized plot of the Fourier transform of the image in (*a*). The doubling of the central row is an artifact of the imaging process, and the centrosymmetry was imposed during computation (the calculation only generates half of the pattern). Arrows 1 and 2 point to spots used in subsequent figures.

Fig. 10 shows composite images that are produced when the patterns described above are superimposed on the original image. Fig. 10(*a*) consists of a simple superposition of Figs. 9(*c*) and 7(*a*). Fig. 10(*b*) corresponds to a more sophisticated treatment, with weighted images from both Figs. 9(*a*) and (*c*) superimposed on Fig. 7(*a*). The origins of the various parts of the image are now more apparent. The small white spots between the tetrahedra can be correlated with the subcell periodicities, whereas the periodicities of the interstrip positions determine the broader superstructure spacings. Additionally, the variations in widths and distribution of the tetrahedral strips become immediately evident. It is these physical changes that reflect local variations in composition and that produce the modulations (Guggenheim & Eggleton, 1986; Ahn & Buseck, 1988).

6.2. *Grossular garnet*

Materials having the garnet structure are widespread in nature and also have great industrial importance. Defect structures have received considerable attention, but their study in detail has been difficult because of the close-packed dense structure of garnet. During a study of anomalous optical properties of grossular garnet ($Ca_3Al_2Si_3O_{12}$) (Allen & Buseck, 1988), we encountered curious dislocation structures (Allen, Smith & Buseck, 1987). Image processing has provided a means for highlighting these dislocations.

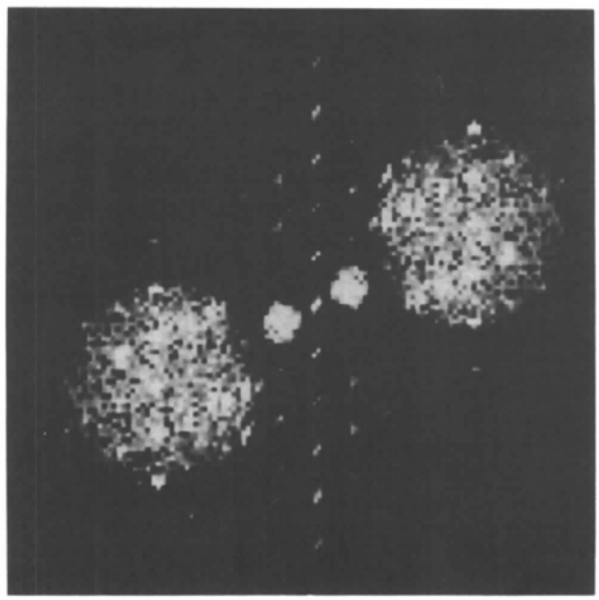

Fig. 8. Superposition onto Fig. 7(*b*) of two pairs of spots from the digitized diffractogram. These spots were generated by paired non-centered filters placed around spots 1 and 2 of Fig. 7(*b*) after the 000 signal was suppressed with a digitized 'beam stop'; this 'stop' enhanced the signals from subcell and supercell spots. Both pairs of filters correspond to the same direction α and same divergence φ.

Fig. 11(*a*) is from Allen *et al.* (1987) and shows partial dislocations and associated dislocation core. The position of the core is emphasized by adjusting the contrast to produce Fig. 11(*b*). The boundary region where Allen *et al.* (1987) suggested that vacancy sites have been occupied to produce a localized 'doubling' of the structure is illustrated in Fig. 12(*a*) and (*b*), for which different diffraction spots in the DFT were selected for imaging to highlight this structure.

7. Discussion

There are several reasons why signal processing of HRTEM images is useful. In some instances there are too many details in the experimental image to permit simple interpretation. Patterns in the image may not be readily apparent without the removal of low- and high-frequency noise and the objective assistance provided by a processed image. The superstructures of minnesotaite provide an example.

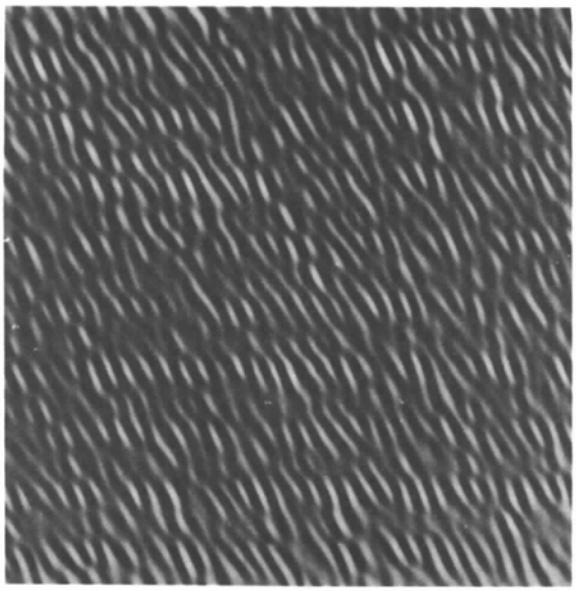

(*a*)

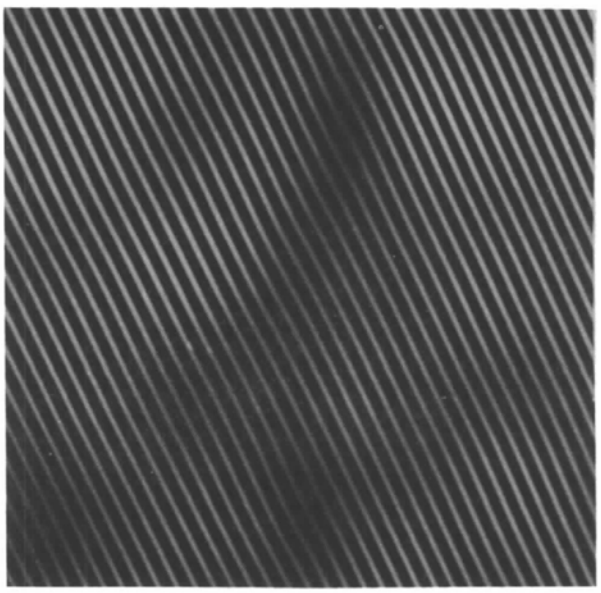

(*b*)

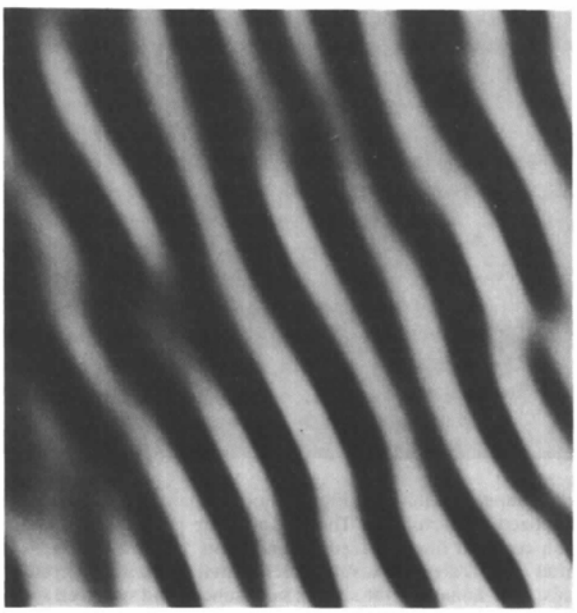

(*c*)

Fig. 9. (*a*) Image produced by using only the large paired signals in Fig. 8. (*b*) Image produced by decreasing the diameters of the apertures used to produce (*a*); the smaller apertures minimize the influence of diffuse scattering. Except for the minor 'clouding', this image shows only the subcell periodicity. (*c*) Image produced by using only the small paired signals in Fig. 8. These broad bands correspond to the positions of the tetrahedra at the interstrip positions. They indicate the relative alignment of the strips, and regions of greater width are prominent. Positions where the interstrip positions are relatively misaligned appear more diffuse.

Digital filters can be used to highlight features of special interest and to explore their distribution and character. This permits a 'dissection' of the diffractogram into its component parts. Since digital filters can be adjusted almost continuously, this procedure allows great flexibility for the study of, for example, features in the diffractogram that are produced by inelastic scattering or by poorly periodic features.

Although of less fundamental interest, addition of false color to the processed signal permits the highlighting of features of special interest for purposes of illustration or display [*e.g. Science* cover (Allen *et al.*, 1987)]. Slides for talks can be prepared and colored to emphasize desired parts of the images.

Once a processed signal is available, different portions of the signal can be separated and then selectively recombined. Such composites are helpful for understanding images such as those produced by minnesotaite.

The presence of linear features such as dislocations can be highlighted, as in the case of grossular garnet, and non-periodic stacking sequences such as occur in graphite, layer silicates and other layered structures can be similarly emphasized. A final use to which these processed images can be put is the comparison between digitized experimental images and their computed counterparts. Bringing different features to roughly uniform levels of contrast should help considerably in evaluating the matches between experimental and computed images.

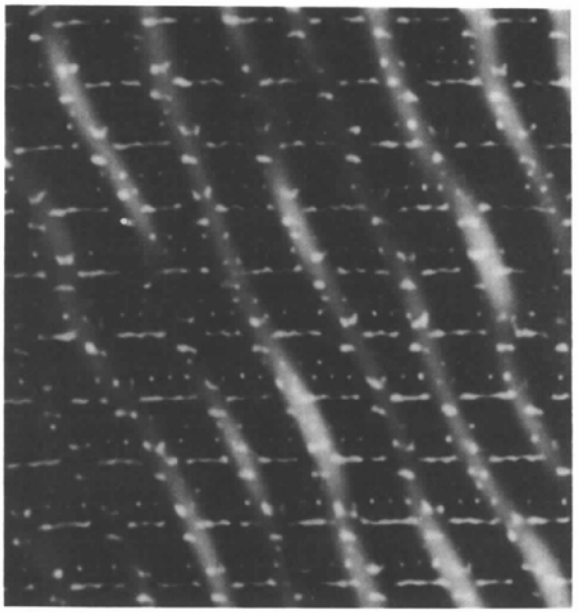

(*a*)

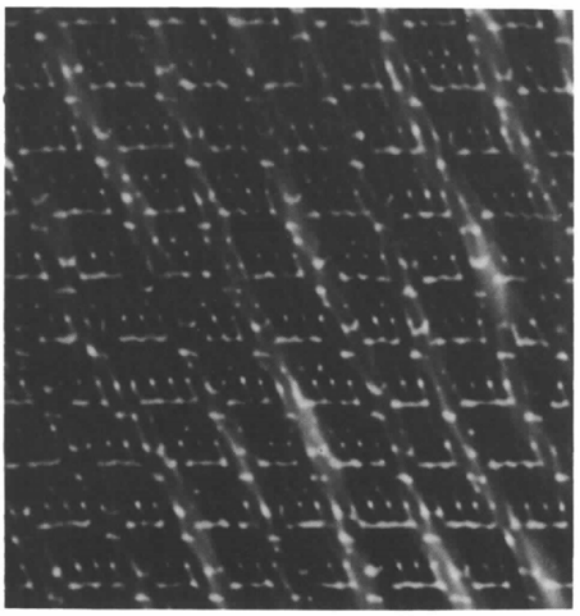

(*b*)

Fig. 10. Composites of images. (*a*) This image, produced from Fig. 9(*c*) superimposed on the original image, confirms that the broad bands of Fig. 9(*c*) correspond to the interstrip tetrahedra. (*b*) This image results from superimposing the images obtained from Figs. 9(*a*) and (*c*) onto that in Fig. 7(*a*). It highlights the subcell periodicity relative to the broader bands at the interstrip sites.

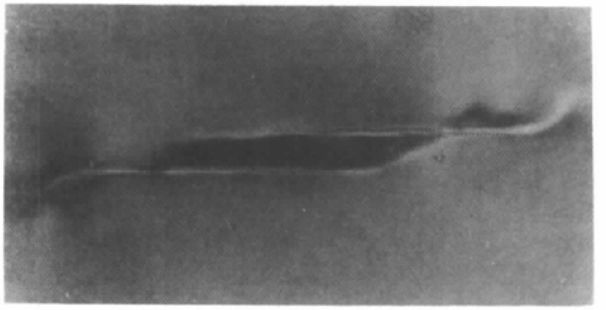

(*a*)

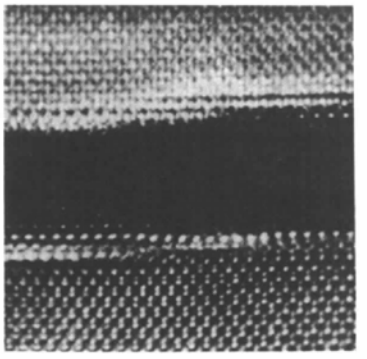

(*b*)

Fig. 11. (*a*) Experimental high-resolution image of grossularite garnet (Allen *et al.*, 1987). The disrupted region in the center is a dislocation core. (*b*) Processed imge from (*a*). It has had its contrast adjusted to emphasize the core region.

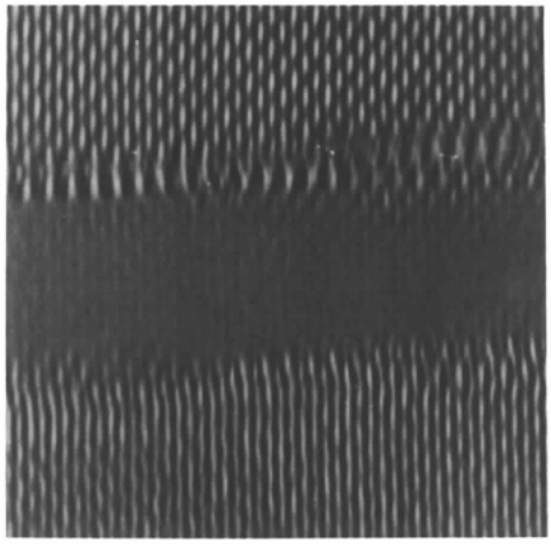

(*a*)

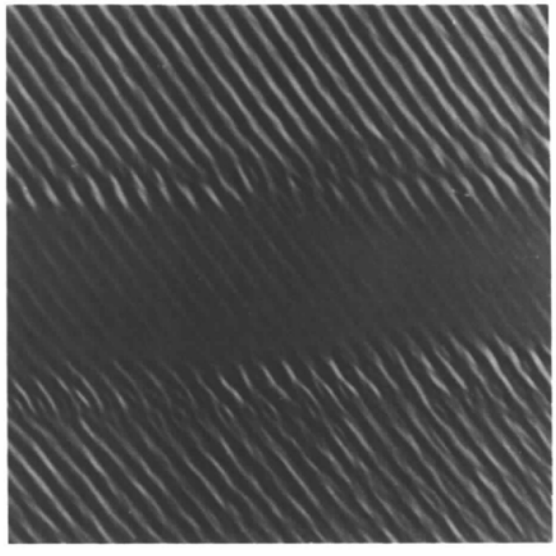

(*b*)

Fig. 12. An elliptical (polarizing) filter has been used to highlight the localized 'doubling' of the structure on the right side, adjacent to and above the core region. In (*a*) the major axis of the elliptical filter is horizontal, whereas in (*b*) the major axis of the ellipse is inclined.

We thank M. A. O'Keefe, P. Rez, D. J. Smith and D. A. Buseck for their helpful comments, J. H. Ahn, J. Barry and F. Allen for their HRTEM images of minnesotaite and garnet, and F. Morris for his help in both mathematical and computing treatments. This work was partly supported by grants EAR8408168 and EAR8708529 from the National Science Foundation (NSF) and by support from the CNRS and the Laboratoire de Minéralogie et Cristallographie. Electron microscopy was done at the ASU Facility for High-Resolution Electron Microscopy, which is funded by grants from the NSF and Arizona State University.

References

AHN, J. H. & BUSECK, P. R. (1988). In the press.
ALLEN, F. M. & BUSECK, P. R. (1988). *Am. Mineral.* **73**, 568–584.
ALLEN, F. M., SMITH, B. K. & BUSECK, P. R. (1987). *Science*, **238**, 1695–1697.
BIJAOUI, A. (1981). *Image et Information.* Paris: Masson.
BRILLOUIN, L. (1959). *La Science et la Theorie de l'Information.* Paris: Masson.
CASTLEMAN, K. R. (1977). *Images and Digital Processing. Digital Image Processing*, pp. 3–13. Englewood Cliffs: Prentice-Hall.
COOLEY, J. W. & TUKEY, J. W. (1965). *Math. Comput.* **19**, 297–301.
FELGETT, P. & LINFOOT, E. H. (1955). *Philos. Trans. R. Soc. London Ser. A*, **247**, 369–372.
GONZALES, R. C. & WINTZ, P. (1977). *Digital Image Processing*, pp. 115–176. Reading, MA: Addison-Wesley.
GUGGENHEIM, S. & EGGLETON, R. A. (1986). *Can. Mineral.* **24**, 479–497.
HOBBS, L. W. (1979). *Introduction to Analytical Electron Microscopy*, edited by J. HREN *et al.*, p. 437. New York: Plenum.
HOBBS, L. W. (1983). 41*st Annu. Proc. Electron Microsc. Soc. Am.* pp. 346–349. San Francisco: San Francisco Press.
O'KEEFE, M. A. & BUSECK, P. R. (1979). *Trans. Am. Crystallogr. Assoc.* **15**, 27–46.
O'KEEFE, M. A., BUSECK, P. R. & IIJIMA, S. (1978). *Nature (London)*, **274**, 322–324.
PRADRE, P., REVOL, J. F. & MANLEY, R. ST JOHN (1987). 45*th Annu. Proc. Electron Microsc. Soc. Am.* pp. 388–389.
RIMSKY, A., EPELBOIN, Y. & MORRIS, F. (1988). In preparation.
SATTLER, M. L. & O'KEEFE, M. A. (1987). 45*th Annu. Proc. Electron Microsc. Soc. Am.* pp. 104–105.
SAXTON, W. O. (1978). *Image Formation Theory. Computer Techniques for Image Processing in Electron Microscopy*, pp. 1–33. New York: Academic Press.
SAXTON, W. O. (1986). 44*th Annu. Proc. Electron Microsc. Soc. Am.* pp. 526–529.
SAXTON, W. O., PITT, T. J. & HORNER, M. (1979). *Ultramicroscopy*, **4**, 343–354.
SHANNON, C. E. (1948). *Bell Systems Tech. J.* **27**, pp. 327, 623.
SMITH, D. J., SAXTON, W. O., O'KEEFE, M. A., WOOD, G. J. & STOBBS, W. M. (1983). *Ultramicroscopy*, **11**, 263.
TOURNARIE, M. (1959). Thèse de Doctorat-ès-Sciences. Univ. de Paris, France.
VEBLEN, D. R. & BUSECK, P. R. (1983). 41*st Annu. Proc. Electron Microsc. Soc. Am.* pp. 350–353. San Francisco: San Francisco Press.
YOKOTA, Y., TOMITA, M., HASHIMOTO, H. & ENDOH, H. (1981). *Ultramicroscopy*, **6**, 313–322.